# Detailed modeling of combustion noise using a computational aeroacoustics model

**By A. Giauque AND H. Pitsch**

## 1. Motivation and objectives

When considering the noise produced by a turbulent flow, there are several methods to describe acoustic sources and propagation with different levels of assumptions (Benoit & Nicoud 2005; Crighton *et al.* 1992; Polifke & Sattelmayer 2003; Ihme *et al.* 2006). Here, in addition to the direct noise generated by the heat release and the associated density changes in the combustor, indirect noise production is considered, i.e., the sound emitted by hot spots traveling through pressure gradients. Indeed, indirect noise is currently seen as one of the main sources of the core noise generated by auxiliary power units in aircraft.

Goldstein's generalized acoustic analogy (Goldstein 2003) is an exact rearrangement of the governing Navier-Stokes equations. The major advantage of this analogy is its expected ability to capture the indirect noise production phenomenon and its applicability in confined geometries.

The main objectives of the present paper are

- Extend Goldstein's acoustic analogy for reactive flows
- Develop an efficient and precise numerical solver for this analogy
- Validate the method with an incompressible or low Mach number LES solver for an academic configuration with indirect noise production
- Study indirect combustion noise in realistic cases using low Mach reactive LES

## 2. Theoretical background

### 2.1. *Extension of Goldstein's acoustic analogy for reactive cases*

In his original article, Goldstein (2003) derived a generalized acoustic analogy for non-reactive flows. Yet, source terms arising from chemical reactions and heat transport by species exist in reactive configurations and must be accounted for. The derivation of the generalized acoustic analogy for the reactive case also requires that thermodymamic quantities such as $C_p$ and $r$ are not assumed constant anymore.

First, the Navier-Stokes equations in conservative form are considered:

$$\frac{\partial \rho}{\partial t} + \frac{\partial}{\partial x_j}\rho v_j = 0 \tag{2.1}$$

$$\frac{\partial}{\partial t}\rho v_i + \frac{\partial}{\partial x_j}\rho v_i v_j + \frac{\partial p}{\partial x_i} = \frac{\partial}{\partial x_j}\sigma_{ij} \tag{2.2}$$

$$\frac{\partial}{\partial t}(\rho h_0 - p) + \frac{\partial}{\partial x_j}\rho v_j h_0 = \frac{\partial q_j}{\partial x_j} + \frac{\partial}{\partial x_j} v_i \sigma_{ij} + \dot{\omega}_T, \tag{2.3}$$

where

$$h_0 = h + \frac{1}{2}v^2 \tag{2.4}$$

denotes the stagnation enthalpy, $h$ the enthalpy, $p$ the pressure, $\rho$ the density, $v$ is the fluid velocity, $\sigma_{ij}$ the viscous stress tensor, $q$ the heat flux vector and $\dot{\omega}_T$ is the heat release. The equation of state is taken to be the ideal gas law

$$p = \rho r T, \qquad h = C_p^\star T, \tag{2.5}$$

where $r = C_p - C_v$ is the gas constant, $C_p$ and $C_v$ are the specific heats at constant pressure and volume of the mixture, $C_p^\star$ is defined by $\sum_k^N Y_k \int_0^T C_{p,k} dT/T$ where $N$ is the number of species in the mixture, and $Y_k$ the mass fraction of the species $k$. $T$ is the absolute temperature. With

$$\rho = \bar{\rho} + \rho', \quad p = \bar{p} + p', \quad h = \tilde{h} + h', \quad v = \tilde{v}_i' + v_i' \tag{2.6}$$

the dependent variables as well as in a similar way the viscous stress tensor $\sigma_{ij}$, the heat flux $q$, and the heat release $\dot{\omega}_T$, are divided into their base flow components $\bar{\rho}$, $\bar{p}$, $\tilde{h}$, $\tilde{v}_i$, $\bar{\sigma}_{ij}$, $\bar{q}$ and $\overline{\dot{\omega}}_T$ and their residual components $\rho'$, $p'$, $h'$, $v_i'$, $\sigma_{ij}'$, $q'$ and $\dot{\omega}_T'$. The overbar operator can denote any averaging operation applied to the flow variables. As an example, if the base flow is statistically stationary, this operator could be the Reynolds averaging operator. On the other hand, if the base flow is unsteady in the mean, the overbar operator can also denote an ensemble average

$$\overline{f} = \lim_{N\to\infty} \frac{1}{N} \sum_{i=1}^{N} f_i(x,t), \tag{2.7}$$

where $N$ is the number of samples.

The tilde operator is defined as the Favre average $\tilde{\bullet} = \overline{\rho\bullet}/\bar{\rho}$. Base flow components are required to satisfy the Navier-Stokes equations

$$D_0 \overline{\rho} = 0, \tag{2.8}$$

$$D_0 \overline{\rho} \tilde{v}_i + \frac{\partial \overline{p}}{\partial x_i} = \frac{\partial}{\partial x_j}\left(\widetilde{T}_{ij} + \overline{\sigma}_{ij}\right), \tag{2.9}$$

$$D_0 \overline{\rho} \tilde{h}_0 - \frac{\partial \overline{p}}{\partial t} = D_0 \widetilde{H}_0 + \frac{\partial}{\partial x_j}\left(\widetilde{H}_j - \bar{q}_j + \tilde{v}_i \bar{\sigma}_{ij}\right) + \overline{\dot{\omega}}_T, \tag{2.10}$$

where the non-linear operator $D_0$ is defined by

$$D_0 f = \frac{\partial f}{\partial t} + \frac{\partial}{\partial x_j} \tilde{v}_j f, \tag{2.11}$$

and

$$\tilde{h}_0 = \tilde{h} + \frac{1}{2}\tilde{v}^2 \tag{2.12}$$

is the base flow stagnation enthalpy. The base flow variables, $\bar{\rho}$, $\bar{p}$ and $\tilde{h}$ are also required to satisfy an ideal gas law equation of state,

$$\tilde{h} = \widetilde{C_p^\star T} = \frac{\overline{C_p^\star p}}{r}\frac{1}{\bar{\rho}}. \tag{2.13}$$

The source "strengths" $\widetilde{T}_{ij}$, $\widetilde{H}_0$ and $\widetilde{H}_i$ are defined as

$$\widetilde{T}_{ij} = -\bar{\rho}\left(\widetilde{v_i v_j} - \tilde{v}_i \tilde{v}_j\right) \tag{2.14}$$

$$\widetilde{H}_0 = \delta_{ij}\frac{1}{2}\widetilde{T}_{ij} \tag{2.15}$$

$$\widetilde{H}_i = -\bar{\rho}\left(\widetilde{h_0 v_i} - \tilde{h}_0\tilde{v}_i\right) - \widetilde{H}_0\tilde{v}_i. \tag{2.16}$$

To obtain the governing equations for the residual variables, substitute Eq. 2.6 into the Navier-Stokes equations (2.1–2.3) and subtract out Eqs. 2.8–2.10 to obtain

$$D_0\rho' + \frac{\partial m_j}{\partial x_j} = 0 \tag{2.17}$$

$$D_0\left(m_i + \rho'\widetilde{v}_i\right) + \frac{\partial m_j\widetilde{v}_i}{\partial x_j} + \frac{\partial p'}{\partial x_i} = \frac{\partial e_{ij}}{\partial x_j} \tag{2.18}$$

$$\begin{aligned} D_0\left(\pi + \mathbf{m}\cdot\tilde{\mathbf{v}} + \frac{1}{2}\rho'\tilde{v}^2\right) - \frac{\partial p'}{\partial t} + \frac{\partial m_j\widetilde{h_0}}{\partial x_j} \\ = -D_0\left(\frac{1}{2}\rho v'^2 + \widetilde{H_0}\right) - \frac{\partial}{\partial x_j}[\rho v_j'\left(h' + \frac{1}{2}v'^2 + \mathbf{v}'\cdot\tilde{\mathbf{v}}\right) \\ +\widetilde{H_j} + q_j' - \widetilde{v}_i\sigma_{ij}' - v_i'\sigma_{ij}] + \dot{\omega}_T', \end{aligned} \tag{2.19}$$

where $m_i = \rho v_i'$, $\pi = \rho h' + \rho'\tilde{h}$ and, $e_{ij} = -\left(\rho v_i' v_j' + \tilde{T}_{ij} - \sigma_{ij}'\right)$.
Within the reactive framework,

$$\pi = \rho h' + \rho'\widetilde{h} = \left(\frac{C_p^\star p}{r}\right)' \tag{2.20}$$

$$\pi = \overline{\beta}p' + \beta'\overline{p} + \left(\beta' p'\right)', \tag{2.21}$$

where $\beta = C_p^\star/r$.

Equations 2.18–2.19 can be simplified by differentiating the quadratic terms on the left-hand sides by parts and using Eqs. 2.8–2.10, Eqs. 2.21 and 2.22

$$D_0 m_i + \frac{\partial p'}{\partial x_i} + m_j\frac{\partial\widetilde{v}_i}{\partial x_j} + \frac{\rho'}{\bar{\rho}}\frac{\partial\tilde{\tau}_{ij}}{\partial x_j} = \frac{\partial e_{ij}}{\partial x_j} \tag{2.22}$$

$$\begin{aligned} D_0\left(\left(\overline{\beta} - 1\right)p'\right) + \frac{\partial m_j\tilde{h}}{\partial x_j} + p'\frac{\partial\tilde{v}_j}{\partial x_j} - \frac{m_i}{\bar{\rho}}\frac{\partial\tilde{\tau}_{ij}}{\partial x_j} \\ = -D_0\left(\frac{1}{2}\rho v'^2 + \tilde{H}_0\right) - \frac{\partial}{\partial x_i}\left(\rho v_i' h_0' + \tilde{H}_i - \tilde{T}_{ij}\tilde{v}_j + q_i' - v_j'\sigma_{ij}\right) \\ +e_{ij}\frac{\partial\tilde{v}_i}{\partial x_j} - D_0\alpha' + \dot{\omega}_T', \end{aligned} \tag{2.23}$$

where

$$\tilde{\tau}_{ij} = \delta_{ij}\bar{p} - \tilde{T}_{ij} - \bar{\sigma}_{ij},$$

$h_0' = h' + \frac{1}{2}v'^2$, and $\alpha' = \overline{p}\beta' + (p'\beta')'$.
These equations can be put into a more transparent form by introducing the new dependent variables

$$p_e' = p' + \frac{1}{\overline{\beta} - 1}\left(\frac{1}{2}\rho v'^2 + \tilde{H}_0\right) \tag{2.24}$$

$$u_i' = \frac{m_i}{\bar{\rho}} = \rho\frac{v_i'}{\bar{\rho}} \tag{2.25}$$

and source strengths

$$e'_{ij} = e_{ij} + \frac{1}{2\left(\overline{\beta}-1\right)}\delta_{ij}\rho v'^2 - \widetilde{T}_{ij} \tag{2.26}$$

$$\widetilde{e}_{ij} = \widetilde{T}_{ij} - \frac{1}{\left(\overline{\beta}-1\right)}\delta_{ij}\widetilde{H}_0 \tag{2.27}$$

$$\eta'_i = -\rho v'_i h'_0 - q'_i + v'_j\sigma_{ij} \tag{2.28}$$

$$\widetilde{\eta}_i = \tilde{H}_i - \tilde{T}_{ij}\tilde{v}_j \tag{2.29}$$

to obtain

$$\overline{\rho}\frac{\overline{D}}{Dt}\frac{\rho'}{\overline{\rho}} + \frac{\partial}{\partial x_j}\overline{\rho}u'_j = 0\,, \tag{2.30}$$

$$\overline{\rho}\left(\frac{\overline{D}}{Dt}u'_i + u'_j\frac{\partial\widetilde{v}_i}{\partial x_j}\right) + \frac{\partial}{\partial x_i}p'_e - \frac{\rho'}{\overline{\rho}}\frac{\partial}{\partial x_j}\widetilde{\tau}_{ij} = \frac{\partial}{\partial x_j}\left(e'_{ij} - \widetilde{e}_{ij}\right)\,, \tag{2.31}$$

$$\frac{\overline{D}}{Dt}\left(\overline{\beta}-1\right)p'_e + p'_e\frac{\partial\widetilde{v}_j}{\partial x_j} + \frac{\partial}{\partial x_j}\overline{\rho C_p^\star T}u'_j - u'_i\frac{\partial\widetilde{\tau}_{ij}}{\partial x_j} \tag{2.32}$$

$$= \frac{\partial}{\partial x_j}\left(\eta'_j - \widetilde{\eta}_j\right) + \left(e'_{ij} - \widetilde{e}_{ij}\right)\frac{\partial\widetilde{v}_i}{\partial x_j}\underbrace{-D_0\alpha' + \dot{\omega}'_T}_{\textbf{New terms}}\,, \tag{2.33}$$

where

$$\frac{\overline{D}}{Dt} = \frac{\partial}{\partial t} + \tilde{v}_i\frac{\partial}{\partial x_i}.$$

Two new terms are found in Eq. 2.33 that are related to the fluctuations of thermodynamic quantities due to changes in temperature, composition of the mixture, and to heat-release disturbances. Also note that the dependent variable $p'_e$ and the source strengths $e'_{ij}$ and $\tilde{e}_{ij}$ are modified compared to the original equations.

## 3. An accurate and efficient solver

### 3.1. *Space and time discretization*

A solver for the set of equations (Eqs. 2.30–2.33) has been developed in the framework of a structured, finite-difference code with staggering in time and space. This code has been developed for accurate DNS and LES computations (Desjardin *et al.* 2007). The GAA equations are solved explicitly in order to avoid excessive communications between processors, which are needed for an implicit solution of the equations. This choice is also motivated by the fact that the acoustic CFL number should not be greater than 1, which makes an implicit solver less attractive. Time is advanced via an optimized Runge-Kutta algorithm developed by Bogey & Bailly (2004). This implementation requires to remove the time staggering of the NGA code. Yet, the advantages of spatial staggering compared to a collocated scheme are retained. This has the advantage that, compared with a collocated formulation, for a given order of accuracy and a specified number of grid points, a bette r transport of acoustic waves is expected.

Different tests have been performed to study the accuracy of the solver depending on the size of the spatial stencil and the number of Runge-Kutta steps. First, harmonic acoustic waves with a different number of points per wavelength are propagated. Figure 1($a$) shows the influence of the size of the spatial stencil on the velocity of propaga-

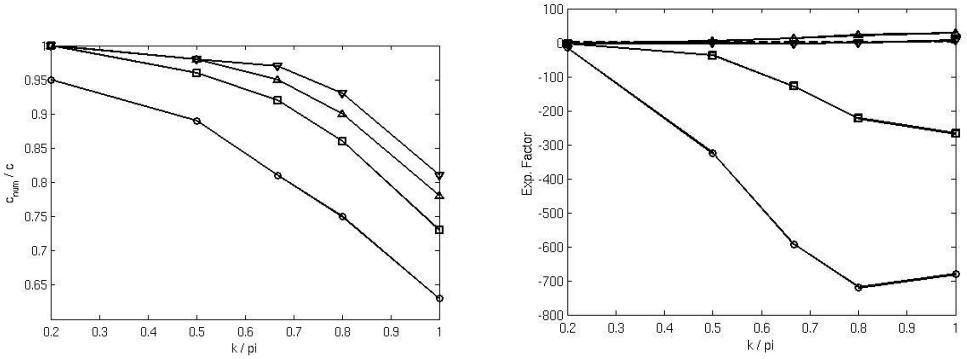


($a$) ($b$)

FIGURE 1. ($a$): Propagation velocity normalized by the speed of sound. Size of the spatial stencil: ○ 2 points □ 4 points △6 points ▽8 points.
($b$): Exponential amplification coefficient of the envelope of the signal. Number of RK steps: – zero amplification ○ 3 steps □ 4 steps △5 steps ▽6 steps

tion. Almost all stencils give the right velocity for $k/\pi$=0.2, which corresponds to a wave discretized with 10 points per wavelength. Yet, differences between the stencils appear as the number of points is decreased. For $k/\pi$=0.5 (i.e., 4 points per wavelength) the 2-points stencil produces a significant error. As expected, for $k/\pi$=1 (i.e., 2 points per wavelength) all orders propagate the acoustic wave with a lower velocity than the speed of sound. But it is important to note that the error is much smaller than with centered schemes (used in collocated formulations), which, as shown by Colonius & Lele (2004 ), tend to have negative propagation velocities as the number of points per wavelength decreases to only 2.

Figure 1($b$) shows the influence of the number of Runge-Kutta steps on the amplification/dissipation of harmonic acoustic waves. This figure shows the exponential amplification coefficient of the envelope of the time signal at a fixed point in the domain. This coefficient should be zero when no amplification/dissipation occurs. Figure 1($b$) shows that small wavelengths are dissipated when using only 3 or 4 steps. Five RK steps amplify short wavelengths. Only the use of 6 RK steps provides a small amplification coefficient. Yet, this coefficient is positive for 2 points per period, which means that these waves tend to be amplified by the solver.

When compared to the results obtained with centered operators (used in collocated formulations) shown in Colonius & Lele (2004), these tests demonstrate the beneficial behavior of the spatial staggering for the propagation of acoustic waves. In order to account for small wavelengths, a number of 6 RK steps should be chosen.

### 3.2. *Temporal and spatial order of accuracy*

To further assess the stability and accuracy of the numerical method, the problem defined by Bogey & Bailly (2004) is computed. The wave propagation equation

$$\frac{\partial^2 p}{\partial^2 t} - c\frac{\partial^2 p}{\partial^2 x} = 0$$

is solved with a time step derived from the mesh spacing as $\Delta t = \mathrm{CFL}\Delta x$. The size of the spatial stencil is given by the number of points used to compute spatial derivatives. Changing the number of RK steps changes the order of accuracy of the discretized

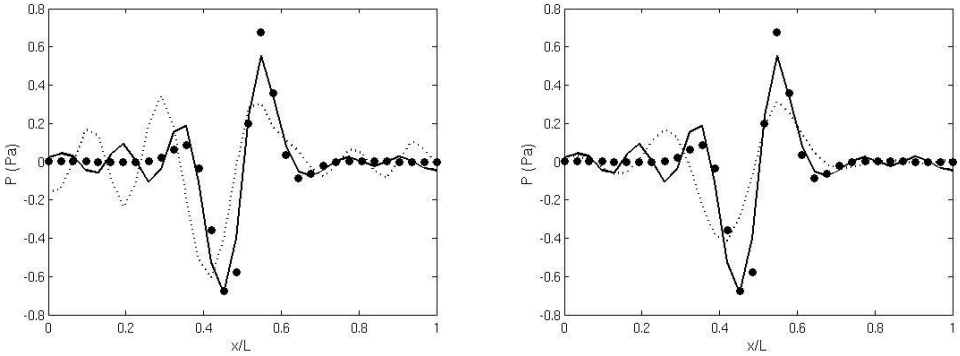


($a$) ($b$)

FIGURE 2. Propagating wave test case: • exact solution; ($a$): spatial stencils: ... 4 points (CFL=0.5), - 6 points (CFL=1.0); ($b$): temporal scheme (CFL=1.0): ... 4 RK steps, - 6 RK steps

time derivative. The initial disturbance has a Gaussian shape wavenumber spectrum, centered around 8 points per wavelength. To study the propagation of this disturbance over a large distance, periodic boundary conditions are implemented in the simulation and comparisons are made between the initial disturbance and after 10 turnover times, which corresponds to a propagation of 40 times the dominant wavelength. This problem will be used to determine the minimal requirements in terms of stencil size, number of RK steps, and use of explicit filtering.

Figure 2($a$) shows the disturbance after 10 turnover times for both the 4-points and the 6-points stencils compared with the exact solution. To perform a fair comparison of the stencils, the computation with the 4-points stencil is performed with CFL = 0.5, whereas CFL = 1 is used for the 6-points stencil. This is done to keep the computational cost almost constant. Six RK steps are used in both cases. The discrete L2 relative error (enum), defined as

$$\text{enum} = \left( \sum \left( p_{\text{calc}} - p_{\text{exact}} \right)^2 / \sum p_{\text{exact}}^2 \right)^{1/2} \tag{3.1}$$

is equal to 0.301 for the 6-points stencil and 0.909 for the 4-points stencil. This shows that at least 6 points are needed to propagate this disturbance over 40 times its dominant wavelength.

Figure 2($b$) shows the disturbance after 10 turnover times from 4- and 6-step RK compared with the exact solution. The CFL is fixed at 1 in both cases and 6 points are used for the spatial stencil. The error enum = 0.737 for the 4-steps RK and enum = 0.301 for the 6-steps RK. Consistently with the earlier results, this shows that 6 RK steps should be used to propagate such disturbances over a large distance.

The 6-steps RK scheme used so far employs of an optimized formulation developed by Bogey & Bailly (2004). This scheme minimizes the temporal dispersion by modifying the RK coefficients. Figure 3 shows that compared to the classical sixth-order scheme, the signal is in better agreement with the exact solution when using the optimized scheme. An error of enum = 0.301 is obtained for the optimized RK, while the error for the classical scheme is enum = 0.391.

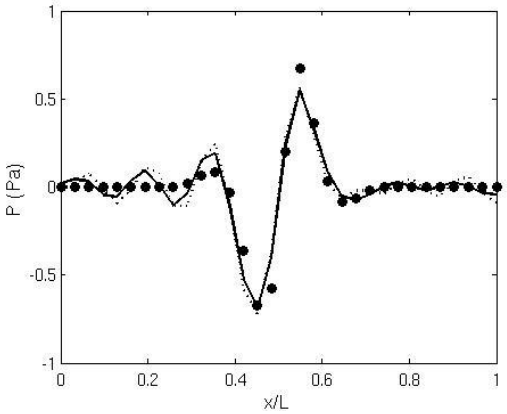


FIGURE 3. Propagating wave test case: • exact solution, CFL=1.0; ... classical 6-steps RK, - optimized 6-steps RK.

### 3.3. *Explicit spatial filtering*

Preliminary tests using harmonic signals show that short wavelengths may be amplified by the solver. To address this issue, a highly selective filter is tested. This filter is designed to damp 4 points or less per wavelength, and keep larger waves unmodified. The damping function of the filter versus $k/\pi$ is shown in Fig. 4. There is a three order of magnitude difference between the amplitude of the damping for 2-points waves ($k/\pi$=1) and 8-points waves ($k/\pi$=1/4), which makes this selective filter almost spectral-like.
To assess the influence of the filter on small wavelengths, a disturbance having a dominant component at 4 points per wavelength is propagated. Figure 5($a$) shows the disturbance after 20 turnover times, which corresponds to a distance of 250 times the dominant wavelength. Without the selective filter, the disturbance is still visible, and although it is not amplified, its spatial spectrum and propagation velocity are wrong. The selective filter damps the major part of the perturbation. Figure 5($b$) shows that this filter has almost no influence on the propagation of the 8-points disturbance, and the numerical error is even slightly decreased (enum = 0.301 with filter, enum = 0.304 without filter).

The numerical scheme selected to solve Goldstein's acoustic analogy includes a 6-points stencil for spatial derivatives and a 6-steps optimized Runge-Kutta for time advancement. A highly selective explicit filter may also be used to damp small wavelengths, that are not well-propagated on the mesh. This combination shows good properties for the computation of acoustic waves down to 8 points per wavelength, even with a unity CFL number.

## 4. Concluding remarks

A numerical solver implementing Goldstein's acoustic analogy has been developed, and preliminary results show that poorly resolved acoustic waves can be accurately propagated as long as both spatial and temporal order of accuracy are at least of order 6. Because of the spatial staggering, to achieve the same accuracy, the required spatial order is divided by 2 compared to a collocated solver. First comparisons with experimental results of noise emissions in a canonical configuration are expected soon.

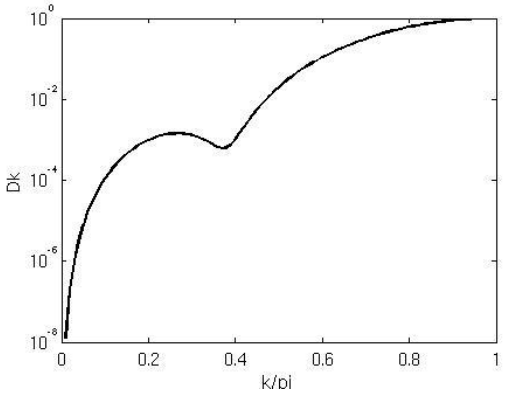


FIGURE 4. Damping function of the selective filter, termed SFo9p in Bogey & Bailly (2004).

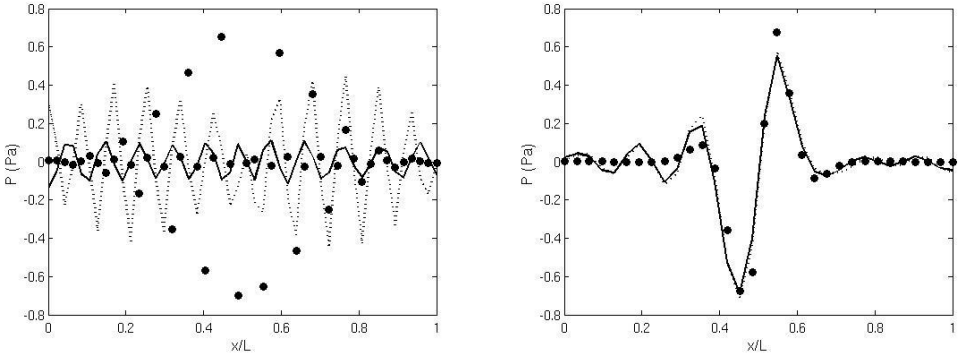


(*a*) (*b*)

FIGURE 5. • Exact solution; (*a*): High-wavenumber propagating wave (CFL=1.0): ... No filtering, - 4th order filtering; (*b*): Propagating wave test case (CFL=1.0): ... No filtering, - fourth order filtering

## 5. Acknowledgments

This work is supported by NASA. The authors thank Dr. Matthias Ihme, Dr. Anne-Laure Birbaud and Christoph Schmitt for many useful discussions.

## REFERENCES

BENOIT, L. & NICOUD, F. 2005 Numerical assessment of thermo-acoustic instabilities in gas turbines. *International Journal for Numerical Methods in Fluids* **47**, 849–855.

BOGEY, C. & BAILLY, C. 2004 A family of low dispersive and low dissipative explicit schemes for flow and noise computations. *Journal of Computational Physics* **194**, 194–214.

COLONIUS, T. & LELE, S. K. 2004 Computational aeroacoustics: progress on nonlinear problems of sound generation. *Progress in Aerospace Sciences* **40**, 345–416.

CRIGHTON, D., DOWLING, A., WILLIAMS, F. J., HECKL, M. & LEPPINGTON, F. 1992 Modern methods in analytical acoustics. *Lecture Notes, Springer Verlag, New-York*.

Desjardin O., Blanquart G., Balarac G. & Pitsch H. 2007 High order conservative finite difference scheme for variable density low Mach number turbulent flows. Submitted to *Journal of Computational Physics*.

Goldstein. M. E. 2003 A generalized acoustic analogy. *J. Fluid Mech.* **488**, 315–333.

Ihme M., Kaltenbacher M. & Pitsch H. 2006 Numerical simulation of flow- and combustion-induced sound using a hybrid LES/CAA approach. *Proceedings of the Summer Program 2006, CTR, Stanford University*, 497–510.

Polifke W. & Sattelmayer T. 2003 Assessment of methods for the computation of the linear stability of combutors. *Combustion science and Technology* **175**, 453–476.